frontiers

Supplementary Material

Intracellular mass density increase is accompanying but not sufficient for stiffening and growth arrest of yeast cells

Shada Abuhattum[1,2†], Kyoohyun Kim[1†], Titus M. Franzmann[3], Anne Eßlinger[3], Daniel Midtvedt[4], Raimund Schlüßler[1], Stephanie Möllmert[1], Hui-Shun Kuan[5,6], Simon Alberti[3], Vasily Zaburdaev[5,6], Jochen Guck[1*]

[1] Biotechnology Center, Center for Molecular and Cellular Bioengineering, Technische Universität Dresden, Dresden, Germany

[2] JPK Instruments AG, Berlin, Germany

[3] Max Planck Institute of Molecular Cell Biology and Genetics, Dresden, Germany

[4] Department of Applied Physics, Chalmers University of Technology, Gothenburg, Sweden

[5] Max Planck Institute for the Physics of Complex Systems, Dresden, Germany

[6]Department of Biology, Friedrich-Alexander Universität Erlangen-Nürnberg, Erlangen, Germany[†] these authors contributed equally to this work

*** Correspondence:**
Jochen Guck
jochen.guck@tu-dresden.de

1 Supplementary Data

1.1 Quantitative analysis of RI tomograms of yeast in different intracellular pH

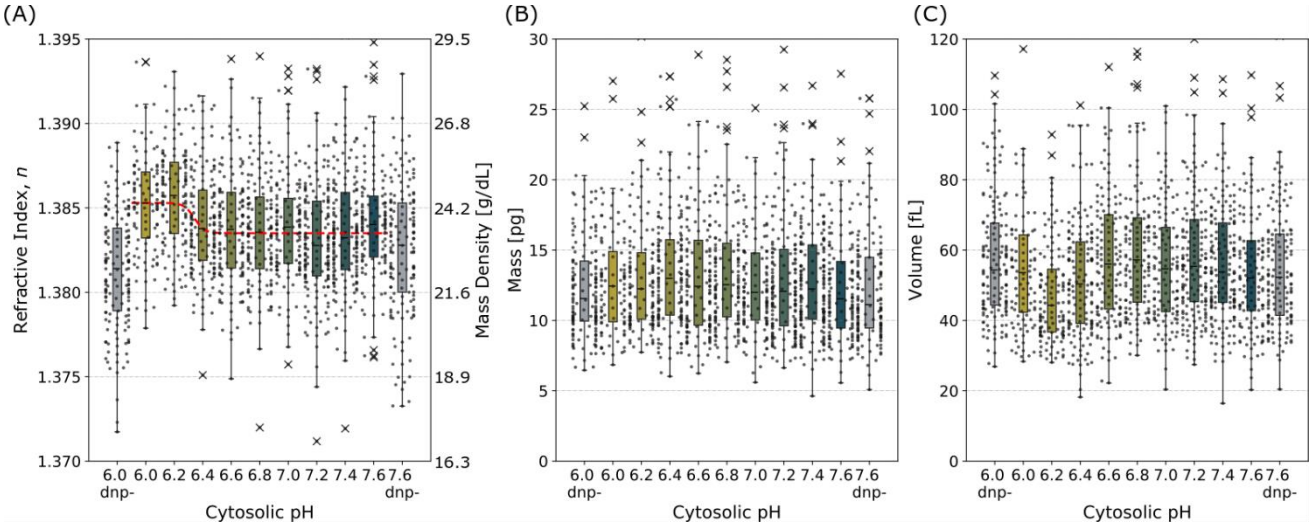

Supplementary Figure 1: The effect of intracellular pH on the refractive index and dry mass of *S. pombe*. The mean refractive index (RI) distribution **(A)**, the dry mass content **(B)**, and cell volume **(C)** of yeast cells at different intracellular pH. The box plot indicates the interquartile ranges (IQR) with a line at the median. The whiskers extend to the data within the 1.5 IQR of the respective quartile. Outliers outside of 1.5 IQR are marked as × (for each condition $N > 95$). The dashed red line in (A) is a sigmoidal fit to the data.

1.2 Isoelectric points analysis for proteins in the *S. pombe* proteome

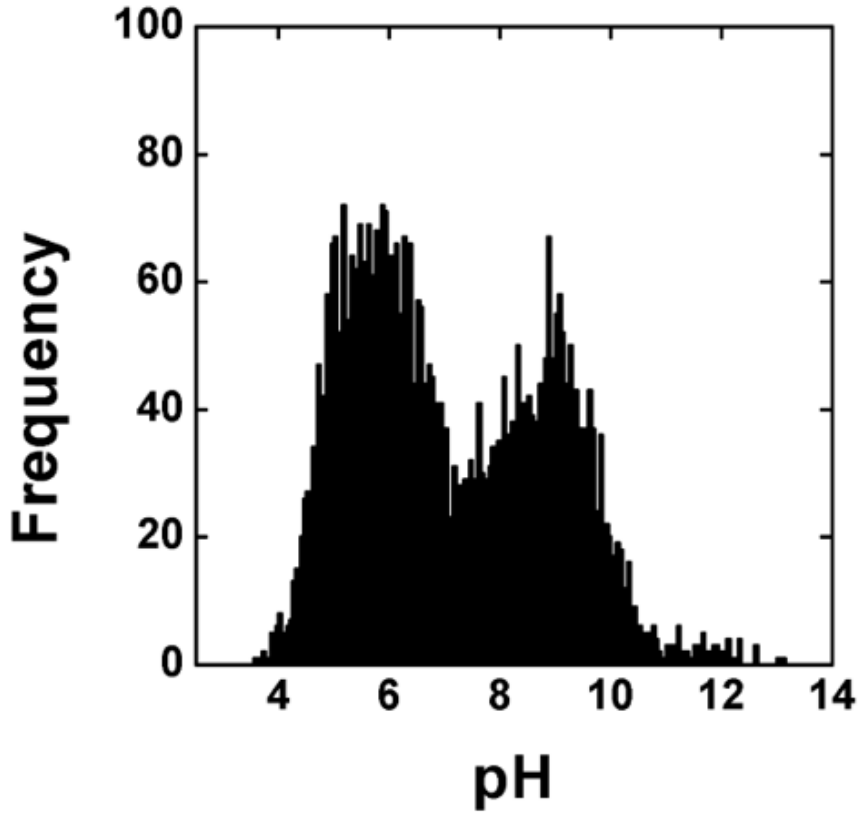

Supplementary Figure 2: Histogram of the isoelectric points of all *S. pombe* yeast proteins, as computed from their primary amino acid sequence (see Munder et al., [1] for details).

2 Supplementary methods:

2.1 Particle tracking in yeast cells with different compression degrees

We compared single-particle tracking data in *S. cerevisiae* cells under three different experimental conditions (cell treated with DNP at an external pH of 7.4, and cells treated with 0.8 M and 1 M sorbitol, respectively). First, the ergodicity of the underlying process was investigated by comparing the ensemble-averaged mean square displacement (E-MSD) to the time-and-ensemble averaged MSD (TE-MSD) [1] For an ergodic process, the statistics of the diffusion process is expected to be invariant under a time-translation, which implies that the E-MSD and TE-MSD are expected to be equal. We find that this is the case for cells treated with DNP and with sorbitol at 0.8 M. For cells treated with 1 M sorbitol the E-MSD was consistently larger than the TE-MSD, indicating a weak breaking of ergodicity in this case (Supplementary Figure 3, TE-MSD shown as dashed line, E-MSD as circles), which may occur, for example, due to intermittent caging effects typically found in glass forming liquids.

Considering that the diffusion of the tracer particles occurs in a complex environment, and that the tracer particle size likely has a rather broad distribution, one may expect their diffusion characteristics to be highly heterogeneous. In order to quantify this, we model the diffusion process by an ensemble of particles each performing fractional Brownian motion (fBm), thus showing time-averaged MSDs

$$\mathrm{MSD}_i(\tau) = K_{\alpha,i}\tau^{\alpha,i} \qquad (1)$$

where $\tau = t/t_0$ is a dimensionless time (t_0 is here an arbitrary time-scale), and K_α has dimension μm^2.

As has been shown in a previous work [1], the fBm model correctly reproduces several key features of the particle motion. In particular, the displacements of the particles show Gaussian statistics, but subsequent displacements show persistent negative correlation.

Subdiffusion of this kind has been observed in previous studies of diffusion in cells[2,3] and hydrogels[4]. The TE-MSD can then be written as

$$\mathrm{TEMSD}(\tau) = E[\mathrm{MSD}_i(\tau)] = E[K_\alpha]E[\exp(\alpha \cdot \log\tau)] \qquad (2)$$

where in the second equality the strength K_α and subdiffusion exponent α were assumed to be independent random variables[5] and $E[\cdot]$ denotes the expectation value. Note that the last factor is just the moment-generating function of the distribution of subdiffusion exponents with parameter $\log\tau$. Taking the logarithm of this expression and performing a cumulant expansion we obtain

$$\log \mathrm{TEMSD}(\tau) = \log E[K_\alpha] + \sum_{n=1}^{\infty} \frac{\kappa_n (\log\tau)^n}{n!} \approx \log E[K_\alpha] + \mu_\alpha \log\tau + \frac{\sigma_\alpha^2}{2}(\log\tau)^2 \qquad (3)$$

where in the last step the cumulant expansion was truncated at the second term, effectively leading to a Gaussian approximation of the distribution of subdiffusion exponents having mean μ_α and variance σ_α^2. Note, that by instead performing the logarithm prior to performing the ensemble average, one obtains the quantity

$$E[\log \mathrm{MSD}(\tau)] = E[\log K_\alpha] + \mu_\alpha \log\tau \qquad (4)$$

which may be used to estimate the average subdiffusion exponent μ_α. Further, we estimate the distribution of the logarithm of the time-averaged individual particle MSDs ($\mathrm{MSD}_i(\tau)$) using a Gaussian kernel density estimator[6]. The corresponding estimated distributions of MSDs for the three conditions considered are shown in Supplementary Figure 3B,D,F together with $\log \mathrm{TEMSD}(\tau)$ (black line in B, black circles in D and F) and $E[\log \mathrm{MSD}(\tau)]$ (red line in B, red circles in D and F) together with a fit to equation (4) (black dashed line in B, black line in D and F). Note that whereas $\log \mathrm{TEMSD}(\tau)$ overestimates the center of the distribution of single-particle MSDs represented in this way, $E[\log \mathrm{MSD}\,(\tau)]$ represents the average particle behavior well.

Note, that by taking the difference of Eq 3 and Eq 4, one obtains

$$\log \mathrm{TEMSD}(\tau) - E[\log \mathrm{MSD}(\tau)] = \log E[K_\alpha] - E[\log K_\alpha] + \frac{\sigma_\alpha^2}{2}(\log\tau)^2 \qquad (5)$$

Consequently, within this model the spread in subdiffusion exponents of single particles, σ_α, can be estimated via this difference, by fitting it to a quadratic expression in $(\log\tau)$. We find that particle diffusion in cells treated with DNP and cells treated with 0.8M sorbitol is well represented by this model, whereas diffusion in cells treated with 1 M sorbitol is not (Supplementary Figure 3C,E), suggesting that the model of heterogeneous fractional Brownian motion may not be applicable in the latter case. Under the three conditions considered, we find for the average subdiffusion exponent and its variation: $\mu_\alpha = 0.67, \sigma_\alpha = 0.2$ (DNP treated cells), $\mu_\alpha = 0.72, \sigma_\alpha = 0.26$ (0.8 M sorbitol) and

$\mu_\alpha = 0.8$, σ_α not defined (1 M sorbitol). Overall, the particle diffusion appears to be qualitatively similar for cells treated with DNP at pH 7.4 and cells treated with sorbitol at 0.8 M. At higher osmotic pressures (1M sorbitol) the mobility is markedly lower, consistent with previous findings[7], but the estimated subdiffusion exponent is somewhat larger. The observation of weak ergodicity breaking in cells treated with 1 M sorbitol may suggest that increased cytoplasmic crowding induces a change in the mechanism of passive intracellular diffusion.

As mentioned above, a hallmark of fBm is the existence of persistent negative correlations between displacements. To study this correlation, we define $C_m(n\tau) = \frac{\langle (x(t+m\tau)-x(t))(x(t+(m+n)\tau)-x(t+n\tau))\rangle}{\langle (x(t+m\tau)-x(t))^2\rangle}$. For fBm, one can show that $C_m(n\tau) = \frac{\tau^\alpha}{2}(2|n|^\alpha - |m-n|^\alpha - |m+n|^\alpha)$. In Supplementary Figure 4, the correlation $C_2(n\tau)$ as defined above is shown for particles diffusing in cells treated with 0.8M (circles) and 1M (squares) sorbitol, respectively. It is clear that the displacements show persistent negative correlations that agree well with the expectation for fBm (see blue and red line for the expected correlation for fBm with $\alpha = 0.72$ and $\alpha = 0.8$ respectively).

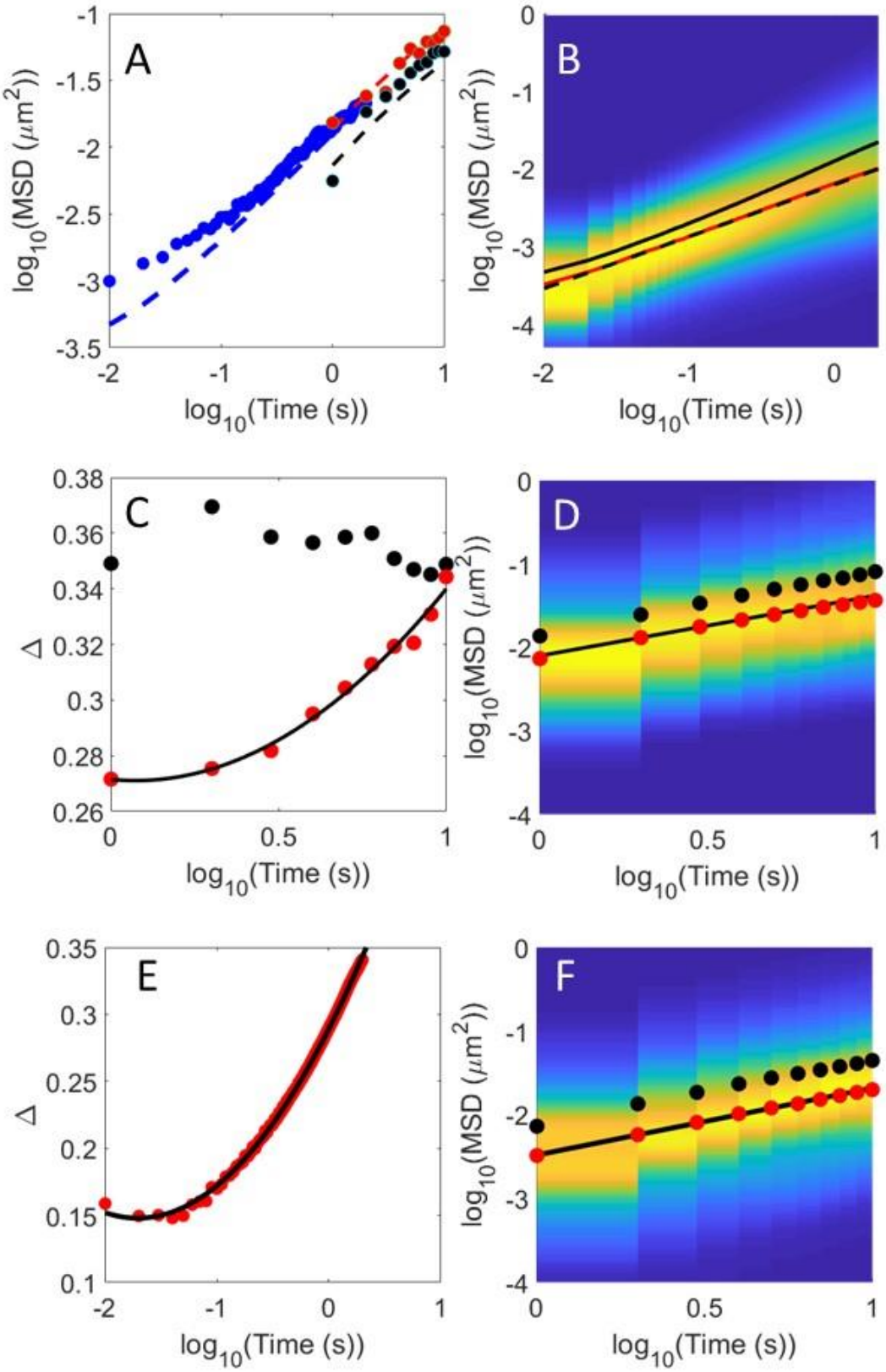

Supplementary Figure 3: Quantification of diffusion in yeast treated with DNP at pH 7.4 or treated with sorbitol at two concentrations (0.8 M and 1 M). (**A**) Time-and-ensemble averaged MSDs (dashed

lines) and ensemble-averaged MSDs (circles) for cells treated with DNP at pH 7.4 (blue), with sorbitol at 0.8 M (red) and at 1 M (black). (**B,D** and **F**) Distributions of individual particle MSD for cells treated with DNP (**B**), with sorbitol at 0.8 M (**D**) and at 1 M (**F**). The TE-MSD are shown as black circles (line for DNP treated cells) whereas $\mathbf{E}[\log \mathbf{MSD}]$ is shown as red circles (line for DNP treated cells). (**C,E**) The difference $\log \mathbf{TEMSD}(\boldsymbol{\tau}) - \mathbf{E}[\log \mathbf{MSD}(\boldsymbol{\tau})]$ for sorbitol treated cells (**C**, with black circles corresponding to 1 M, and red circles to 0.8 M together with a best fit to the 0.8 M data (black line)) and DNP treated cells (**E**, with a best fit shown as black line).

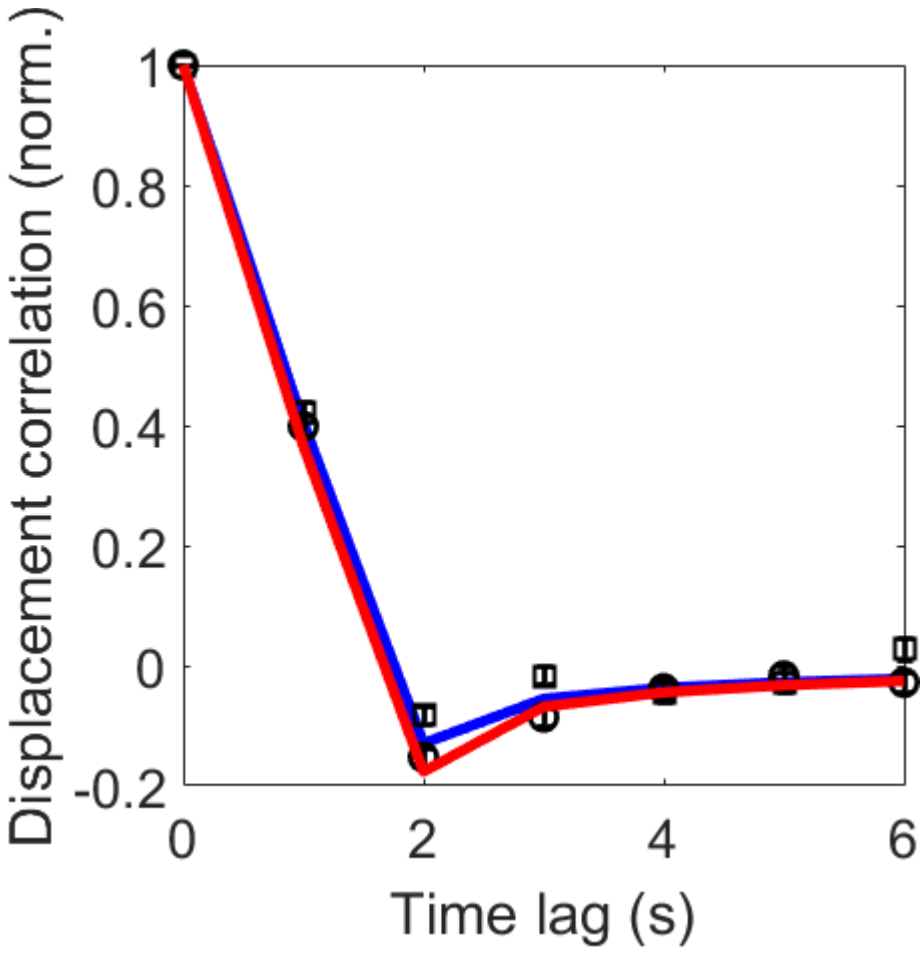

Supplementary Figure 4: The normalized displacement correlation (defined in text) as a function of lag time for yeast cells treated with 0.8 M sorbitol (circles) and 1 M sorbitol (squares). The measured correlations are compared to the theoretically expected correlations for fBm with $\boldsymbol{\alpha = 0.72}$ (blue line) and $\boldsymbol{\alpha = 0.8}$ (red line).

References

1. Munder MC, Midtvedt D, Franzmann T, Nüske E, Otto O, Herbig M, Ulbricht E, Müller P, Taubenberger A, Maharana S, et al. A pH-driven transition of the cytoplasm from a fluid- to a solid-like state promotes entry into dormancy. *eLlife* (2016) **5**:1–30. doi:10.7554/eLife.09347

2. Tejedor V, Bénichou O, Voituriez R, Jungmann R, Simmel F, Selhuber-Unkel C, Oddershede LB, Metzler R. Quantitative analysis of single particle trajectories: Mean maximal excursion method. *Biophys J* (2010) doi:10.1016/j.bpj.2009.12.4282

3. Jeon JH, Tejedor V, Burov S, Barkai E, Selhuber-Unkel C, Berg-Sørensen K, Oddershede L, Metzler R. In vivo anomalous diffusion and weak ergodicity breaking of lipid granules. *Phys Rev Lett* (2011) doi:10.1103/PhysRevLett.106.048103

4. Stempfle B, Große A, Ferse B, Arndt KF, Wöll D. Anomalous diffusion in thermoresponsive polymer-clay composite hydrogels probed by wide-field fluorescence microscopy. *Langmuir* (2014) doi:10.1021/la503571j

5. Kepten E, Bronshtein I, Garini Y. Improved estimation of anomalous diffusion exponents in single-particle tracking experiments. *Phys Rev E - Stat Nonlinear, Soft Matter Phys* (2013) doi:10.1103/PhysRevE.87.052713

6. Silverman B. Density estimation for statistics and data analysis. *Chapman Hall* (1986) doi:10.2307/2347507

7. Miermont A, Waharte F, Hu S, McClean MN, Bottani S, Leon S, Hersen P. Severe osmotic compression triggers a slowdown of intracellular signaling, which can be explained by molecular crowding. *Proc Natl Acad Sci* (2013) doi:10.1073/pnas.1215367110